

TECHNOLOGY DEMONSTRATOR OF A ROCKET CARRYING A DEPLOYABLE FLEET OF AUTONOMOUS GLIDERS

Patrick Spieler

Swiss Federal Institute of Technology, Lausanne, Switzerland, patrick.spieler@alumni.epfl.ch

Elena Sorina Lupu, Dalmir Hasic, Michael Spieler, Michael Pellet, Hassan Arif, Cyril Baumann, Quentin Talon, Emilio Lozano

Swiss Federal Institute of Technology, Lausanne, Switzerland

Oliver Kirchhoff, Laurent Jung

Swiss Federal Institute of Technology, Zurich, Switzerland

Stephane Teste

John Hopkins University, United States of America

Christian Cardinaux

Western Switzerland University of Applied Sciences - HEIG-VD, Switzerland

Dr. Anton Ivanov, Prof. Dario Floreano, Dr. Stefano Mintchev

Swiss Federal Institute of Technology, Lausanne, Switzerland

The Intercollegiate Rocket Competition (IREC) gathers students across the world to design and build a rocket that reaches an altitude of 10,000 ft (approximately 3 km) or 30,000 ft (approximately 9 km). The rocket needs to carry 8.8 lb (4 kg) of payload. As a part of this competition, team DUSTER, formed by students from three Swiss universities designed and built a rocket targeting an apogee of 3 km. The rocket's propulsion system is a Commercial-Off-The-Shelf solid motor. Custom avionics inside the rocket nosecone log and transmit telemetry back to the ground, control the ejection of the nosecone and the payload deployment. A payload is placed in the rocket. This payload consists of an autonomous glider that is ejected at apogee. The technology behind both the rocket and the payload, together with concepts for this year's glider and future autonomous fleet of gliders, are presented in this paper. The design process and manufacturing, along with tests done and issues faced over the course of the project are also outlined along with the solutions and recommendations for future iterations.

I. INTRODUCTION

Spaceport America Cup (formerly entitled Intercollegiate Rocket Competition (IREC)) gathers students from all over the world to participate at one of the biggest rocket competitions in the world. Students are launching solid, liquid, and hybrid rockets to target altitudes of 10,000 feet (3048 meters) and 30,000 feet (9144 meters), carrying 8.8 lb (4 kg) of payload. The teams are scored according to the flight performance on the competition day, technical implementation, the quality of the report and research done as a part of the project.

Team DUSTER, representing several Swiss universities, entered this contest to build a solid motor rocket flying to an apogee of 10,000 ft. The main objective of the rocket is to achieve an apogee of 10,000 ft as accurately as possible. Deviations from this

apogee result in point loss in the flight performance¹ category, as following:

$$P = 350 - \frac{350}{2000} * |apogee_{target} - apogee_{actual}| \quad [1]$$

The rocket is designed to follow a dual-event recovery process. The first event is the rocket separation at apogee, after which the rocket descends rapidly on a drogue parachute. The second event happens at 457 meters, which is the release and opening of the main parachute. At the apogee, shortly after separation another two other events occur: first the ejection of the nosecone followed by the payload release.

In the model flown at this year's competition, no control mechanisms were in place and also no air brakes were installed meaning once the rocket is launched the trajectory cannot be influenced. This increased the importance of simulation, as the only

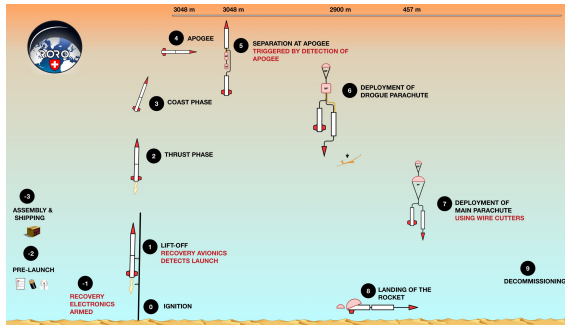


Fig. 1: Concept of Operations for rocket flight

way to determine the altitude the rocket can obtain with a chosen motor and assuming weather conditions. The trajectory of the rocket was simulated in 3 varying environments, including our own developed simulator.²

The second main component of the project is the payload consisting of a glider deployed at apogee. On long-term, our team wants to implement a fleet of gliders deployed from the rocket.

The structure of this paper is as follows: in Section 2 the rocket is presented together with 4 main subsystems: structure, avionics, propulsion and recovery. Section 3 covers the design and technology used in a glider and presents a concept of a fleet of gliders. Navigation and control, one of the main challenges in glider design, are briefly discussed in Section 3.3. The last part (Section 4.1) contains the flight tests of the rocket and the glider. This part is followed by the conclusion and the outlook.

II. ROCKET

The rocket, entitled RORO I, is a 8 feet (2.45 meters) rocket propelled by a M-class solid motor. The main requirements of the rocket are presented in Table 2.

II.i Design and Manufacturing

The rocket is divided into 3 main sub-assemblies (Figure 2):

1. The nosecone - containing avionics, the locking system for the nosecone and its ejection system
2. Upper Body - carrying the payload, the parachutes and the recovery electronics
3. The Lower Body - containing ballast (tungsten), logging avionics and the motor

The rocket was designed to be robust and simple to manufacture due to the time constraints we had. The

The rocket shall achieve an apogee of 10,000 ft (3048 meters).
The rocket shall have be statically stable, but not over-stable.
The rocket shall carry a COTS barometric pressure altimeter with on-board storage to record the altitude.
The launch vehicle shall follow a "dual-event" recovery.
The rocket shall carry a minimum mass of 8.8 lb (4 kg) as payload.
The rocket shall eject its nosecone at apogee.
The rocket shall release a glider from the payload section 5 seconds after apogee.

Table 1: Top Level Requirements for the rocket

rocket separates in the middle, between the upper and lower body to release the parachutes. Before separation the two body tubes are connected using a coupler tube. This approach is very common in High Power Rocketry (HPR) and was chosen to minimize risk.

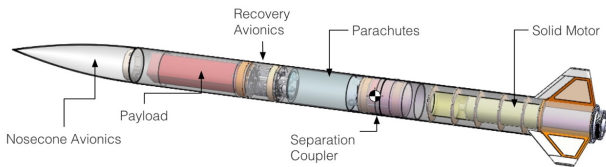


Fig. 2: The rocket with its main components

The length as well as the diameter of the rocket were chosen to accommodate the payload which had a dimension constraint imposed by the competition and the other subsystems.

Next, the manufacturing of each subsystem of the rocket is discussed.

Structure

The main body of the rocket is a COTS phenolic tube, reinforced with two layers of 245 g/m² twill weave carbon fibre. The reinforcement rational is determined using FEA (Finite Element Analysis), and tested during two rocket flights. The structure contains also a coupler tube, that is made out of phenolic tube reinforced inside again with two 245 g/m² layers carbon fibre. The role of the coupler tube is to connect the Lower Body with the Upper Body. The rocket has two structural bulkheads, one in the lower body and one in the upper body to which the parachute cords are attached. The bulkheads are made out of two 15mm plywood plates reinforced

with 4 layers of 245 g/m^2 carbon fibre on each side. The bulkheads are the structurally critical elements as they transfer loads from the rocket body to the subsystems. They need to withstand both the accelerations from the launch and the parachute opening shock. The two bulkheads are subject to a peak load of 10kN from the parachute opening shock. An FEM analysis taking into account the ECSS-E-HB-32-21A³ revealed that an additional reinforcement of the bulkheads with carbon fibre is required to sustain the loads. The analysis of the bonding to the rocket body reveals sufficient strength to sustain the opening shock.

Fins

The fins are sized for 1.1 calibres static stability margin before liftoff. With the burn of the motor and the corresponding mass loss the static margin increases to about 1.8 calibres. After the first test launch and a problem with thrust alignment of the COTS motor described in section 4.1 we decided to increase the fin size in order to increase static stability.

The fins are manufactured out of wood and carbon fibre. The process is shown in Figure 3. Firstly, the wood is cut at CNC (Figure 3 a). The inside of the fins is made out of balsa wood (Figure 3 b), in order to decrease the weight for higher resonance frequencies. Afterwards, on each side of each fin, 3 layers ([span, chord, span] fibre orientation) of 140 g/m^2 unidirectional carbon fibre are applied, to increase stiffness (Figure 3 c). The fins are attached to the motor tube using high temperature epoxy, reinforced with carbon fibre.



Fig. 3: a) Wood at CNC b) Final wood-made fins c) Carbon fibre manufacturing d) Final version of the fins.

Motor tube

The motor tube consists of a COTS phenolic tube. The fins are glued with 3M DP760 high-temperature epoxy to the motor tube. The tube is centred to the outer rocket body tube by six 4mm plywood centring rings distributed in equally along the motor tube. In front of the fins, there is a 12mm CNC-cut plywood ring from which 12 M3 threaded rods connect to the

thrust plate. These help holding the motor inside the rocket body during parachute opening shock. The entire assembly can be seen in Figure 4 c. The fins are fixed to the outer structure using ribbons of carbon fibre both on the inside and the outside of the tube, as it can be seen in Figure 4 a,b.

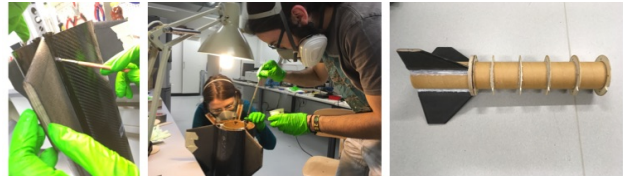


Fig. 4: a, b) Reinforcement of the fins c) Motor tube assembly, with fins and centring rings

Motor case

The motor case, which is a RMS-98/7680 from Aerotech is held by a 98mm retainer from Aeropack on a custom made laser-cut aluminium thrust plate. The thrust-plate pushes directly on the fins which go through the body tube to the motor tube. The thrust-plate is used to attach the motor and hold it when parachute opens. The retainer & thrust-plate assembly can be seen in Figure 5.

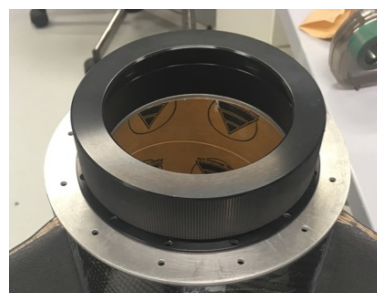


Fig. 5: Motor Retainer and the Aluminum plate

Payload

In the lower body of the rocket, there is 1U of payload consisting of 4kg of tungsten and a board with sensors used to track the lower body motion and shocks. A Gopro and a small camera are also placed to film the parachute deployment and the exterior. The Active Payload bay, placed in the Upper Body, consists of a 4U plywood box reinforced with glass fibre to withstand the loads. Inside the 4U wood box, a glider is mounted on a rail. Shortly after apogee, the glider will be ejected from the rocket using a spring. A description of the glider will be detailed in Section 3.

II.ii Recovery

This subsystem implements a dual-event recovery concept of operations (CONOPS) with an initial deployment event at apogee and a main deployment event at 457 m (1500ft) AGL. Figure 6 illustrates the recovery CONOPS.

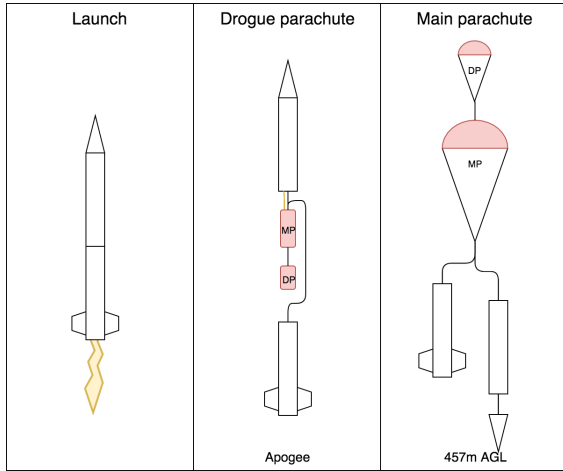


Fig. 6: Recovery CONOPS

During the initial deployment, the rocket is separated and a drogue parachute is released to stabilize the attitude and reduce descent rate to 23-46 m/s (75-150ft/s). At 457 meters AGL, the main deployment takes place where the main parachute is released from the parachute bag to reduce the rocket's descent rate to less than 9m/s (30ft/s) to prevent excessive damage upon impact. Recovery Avionics system triggers the deployment events when the preprogrammed deployment conditions are met by firing a pyrotechnical charge.

Initial Deployment System

The initial deployment is achieved by creating a pressure in the parachute bay and thus forcing the two rocket bodies to separate. The pressure is generated by puncturing a 23 ml CO₂ cartridge by a 0.2 ml black powder charge. The charge forces a puncture piston inside the cartridge seal to release the gas. This system is a COTS solution from Tinder Rocketry Recovery Solutions. There are two redundant CO₂ deployment systems each connected to two igniters. Two redundant recovery electronic components are in charge of triggering the system and each of the two can trigger both systems.

Main Deployment System

The main parachute is stowed in the bag below the drogue parachute. The main parachute is held to-

gether by a wire which is cut at the programmed altitude. Then the load of the rocket pulls the main parachute out of the parachute bag. The setup is illustrated in Figure 7. The wire is cut by a shearing piston which is forced through the wire by a 0.1 ml black powder charge. Two wire cutters are installed for redundancy, one per recovery electronics.

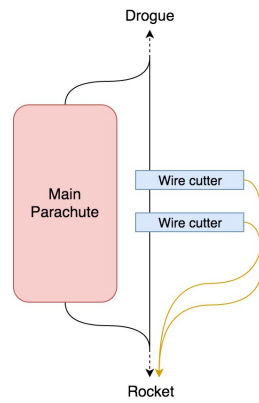


Fig. 7: Main Parachute Deployment

Recovery Avionics

The Recovery Avionics is designed for maximal reliability and features several levels of redundancy which is shown in Figure 8. As required by the competition rules, two redundant electronic systems are used, both of which are different COTS solutions. The pri-

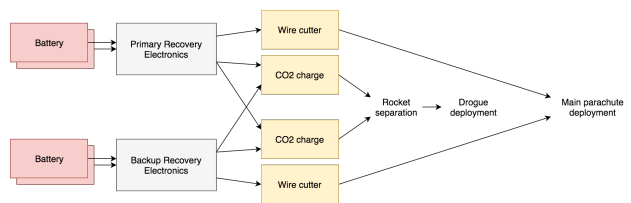


Fig. 8: Recovery Avionics Schema

mary electronics is the AltimaxG3 from Rocketronics which features barometer and accelerometer sensors to estimate the altitude of the rocket. It uses a Kalman filter to estimate acceleration, speed and altitude of the rocket. This is a more robust solution especially when pressure fluctuations can be expected at a high velocity. The backup electronics is the Raven3 from Featherweight Altimeters. The primary electronics is programmed to detect the apogee and fire the two CO₂ charges one after the other with a delay of 0.5 seconds. Then during descent it monitors air pressure until the main parachute deployment altitude is reached and initiates the deployment by

using the wire cutter. The backup electronics is programmed as a timer to trigger the initial deployment after the predicted time to apogee from simulations. During descent it also detects the target altitude using a pressure sensor to trigger the main deployment

Recovery Bay The recovery structure is made out of laser cut and milled plywood glued together with epoxy. It is screwed onto a circular bulkhead glued into the upper rocket tube. The connection to the parachute bay is made as airtight as possible by sealing holes with glue and using rubber washers. Figure 9 shows the assembled recovery bay.

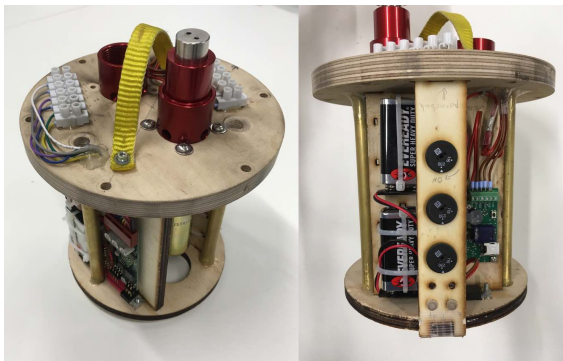


Fig. 9: Recovery Bay

II.iii Avionics

As the rocket body is made of carbon fibre, the only RF transparent part of the rocket is the nosecone (made of fibre glass). Therefore, avionics components were placed there. The avionics consist of 2 PCBs stacked together. The first one, referred to as the **Interface Board (IB)** shown in Figure 10, is equipped with:

- an absolute pressure sensor for altitude measurement
- 2 differential pressure sensors for the Pitot tube
- an IMU
- a microcontroller (STM32F4 of STMicroelectronics)
- a GNSS receiver
- XBee for telemetry downlink to the ground station
- 64 MB of flash memory for data logging
- interfaces such as 2 RS232 ports and USB port

The second PCB, the so called **Power Board (PB)** shown in Figure 11, is equipped with a voltage regulator that power all the nosecone avionics and up to 6 servo outputs.

The decision to split the avionics into 2 PCBs is made to overcome the limited space available and to avoid issues due to EMC. The buck converter on the PB can potentially generate a lot of EM perturbations, thus the sensitive parts such as the GNSS are placed away from it, namely on the IB.

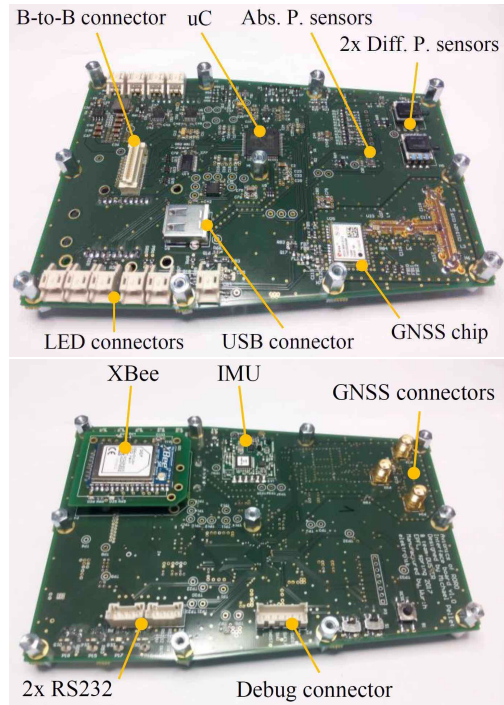


Fig. 10: Interface Board (IB) Top and Bottom)

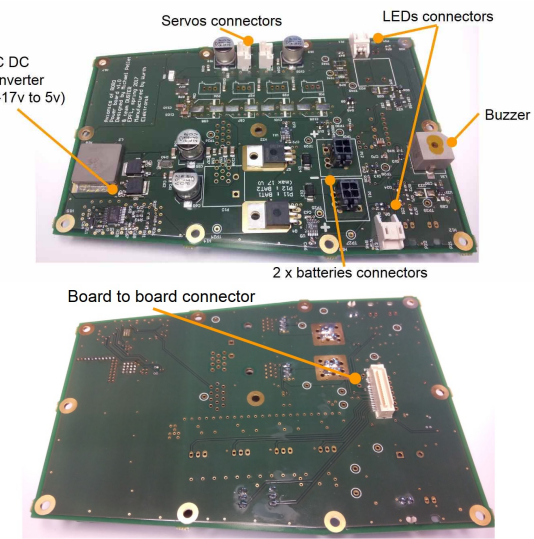


Fig. 11: Power Board (PB) Top and Bottom

Sensors

The Pitot tube uses 2 differential pressure sensors of Honeywell in parallel with different pressure range (0 to 6890Pa and 0 to 103350 Pa). This allows reduction of uncertainties at low speed (uncertainty of 6 m/s at 10 m/s) and ensures good performances at higher speed (uncertainty of 2m/s at 280m/s). The IMU (3 Space High-G of Yost Labs) which is directly soldered on the IB can measure acceleration up to 24g and rate of turn up to 2000/s. By using its integrated data possessing unit, it can directly output orientation (Euler angles, quaternions or rotation matrix) as well as acceleration, rate of turn, magnetic field and velocity increments with a data rate of up to 250 Hz.

The GNSS chip is a NEO-M8T of uBlox equipped with a SAW (surface acoustic waves) filter. As the telemetry antenna (XBee) is close to the 1st GNSS antenna, 2nd SAW filter (SF1186G of muRata) is placed just before the RF input in order to ensure an optimum operation of the GNSS (e.g. avoid jamming due to the XBee frequencies). There are 2 GNSS active antennas. One is placed at the back of the nose cone and is oriented toward the back of the rocket and the other one is placed at the front of the nose cone and is oriented toward the front of the rocket. The 2 GNSS active antennas are controlled via an RF switch on the IB. The first GNSS antenna is used during ascend of the rocket while the second one is used during the descent, after the deployment of the drogue parachute and the nosecone ejection.

Telemetry Downlink

For the telemetry downlink, a 900MHz XBee (XB9X-DMUS-001 of Digi International) is placed on the IB and connected to a 2.1dBi omni antenna. Second XBee is directly connected to the ground station which uses a high gain Yagi antenna (23dB) that is manually oriented towards the rocket during flight. This configuration ensures a good power margin (45dBm) above the sensitivity level of the receiver when at maximum theoretical distance (5 km). The XBee on the IB is fixed with 2 screws and is easily accessible and replaceable in order to replace it according to the country of operation (868 MHz for CH and 900 MHz for the US). Using XBee at 2.4GHz (which is legal for both CH and US) was not an option as they do not have a sufficient communication range.

Actuators

The PB is equipped with 6 servo outputs, each allowing to control a high power servo. These outputs could be used in the future to implement an active control system of the rocket. In RORO I, 2 of these

outputs are used. One is used to control the mechanism which ejects the nosecone while the other is used to control the release of the payload (the glider).

Power Supply

A high power buck converter from Texas Instrument is implemented on the PB. This device allows to power the avionics with 5 VDC with up to 15 A with 2S to 4S (6V to 17V) LiPo batteries. The PB is also equipped with 2 ideal diodes IC that allow to use 2 batteries in parallel for redundancy. In the case of RORO I, 2 3S, 1800 mAh LiPo are used.

Mechanical Design and Manufacturing

Mechanical Integration of the Avionics in the Nosecone

The mechanical structure is designed with the idea of having the avionics easily accessible on the field. The 2 avionics PCBs are staked between 2 CNC machined plates of 3 mm tick plywood and fixed together with PCB spacers. On each plywood plate, gliding structures made out on plywood are glued. This assembly, called the avionic drawer (AD), can be easily slided into the avionic rack (AR) which is a structure made of several parts of CNC machined 6 mm tick plywood fixed to the control panel. To secure the AD, the aluminum GNSS ground plane of the 1st GNSS antenna is fixed on the top of it with nuts to two M5 threaded rods. These 2 threaded rods pass trough the avionic rack and are fixed to the control panel. On the control panel side, a hook is fixed at the end of each threaded rod. These hooks are used to fix the rope that link the nosecone to the upper body bulkhead. The structure made of the control panel on which the AR together with the AD is fixed can be slided into the nosecone and be fixed with 6 M3 screws to a plywood crown glued with epoxy to the nosecone. The Avionics Bay inside the nosecone is depicted in Figure 12.

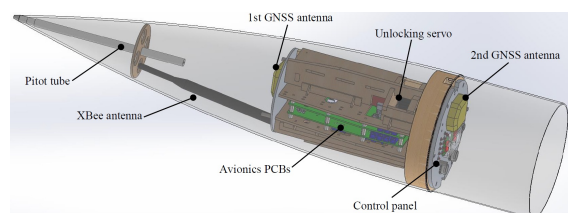


Fig. 12: Avionics Bay inside the Nosecone

Nosecone Deployment System

Note: in the following paragraph, everything noted in parenthesis refers to the Figure 13

In order to get the satellite fix for the GNSS after apogee, the nosecone needs to be deployed. Moreover, this makes an opening in the upper body that allows to deploy the payload. So, to ensure the deployment of the nosecone, an ejection system was designed and manufactured that take into account the fact that the main part of the volume below the nosecone is occupied by the payload.

The designed and manufactured system consist of 2 aluminum U-profiles (6.) fixed to the bulkhead (2.) of the upper body (1.). At the upper end of the u-profiles, a hook is fixed (7.) that is used by the locking system to secure the nosecone (5.). A gliding structure (3.) made out of 2 bigger aluminum U-profiles joined together with 4 arcs cut out of a phenolic tube can slide into the upper body. In the smaller U-profiles (6.), a traction spring (4.) is fixed just bellow the hook (7.), the other end of the spring is fixed on the gliding structure (3.). So, when the nosecone is put in place, the upper part of the gliding structure comes in contact with the lower end of the nosecone and, thus, the gliding structure is pushed in the upper body which loads the 2 springs. When fully loaded, the 2 spring produce a total force of c.a. 100N. When the nosecone is released (thanks to the locking system) the gliding structure pushes it away from the upper body.

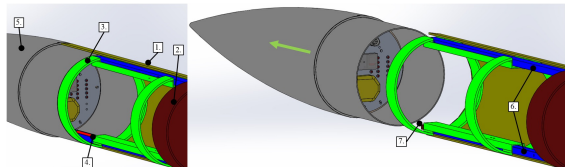


Fig. 13: Deployment System of the Nosecone. LEFT: In place on the upper body. RIGHT: after deployment. (for clarity, payload is not shown)

Nosecone Locking System

Note: in the following paragraph, everything noted in parenthesis refers to the Figure 14.

To secure the nosecone in place during the ascend of the rocket, a locking system was designed and manufactured. This system consist out of 2 steel pins of 6 mm diameter (2. and 3.) loaded with a compressive spring (4.) that can slide in a structure (1.) fixed to the control panel of the nosecone. An inverted came wheel (5.) controlled with a servo that is fixed to the AR is used to move the 2 pins forth and back. When locked, the end of the 2 pins goes in a hook (7.) fixed to each outer rail (6.) of the deployment system. When unlocked, the steel rods are retracted and

comes out of the hooks. This configuration, with an inverted came wheel, allows to unlock the nosecone from the outside even if there is a failure of the servo or the avionics. Indeed, the axis of the 2 locking steel rods is aligned with the 2 holes (8.) made in the nosecone for Pitot tube's static pressure measurement, thus, the locking system can be unlocked using 2 screwdriver to push the pins inside the nosecone

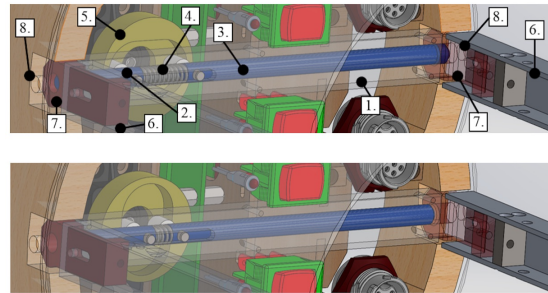


Fig. 14: Locking System of the Nosecone. Top: locked, Bottom: unlocked

III. GLIDERS

III.i General Overview

Each team can choose an arbitrary payload to be placed in the rocket. The team decided to develop long-term a set of gliders that are, once deployed from the rocket, flying back to the ground in formation.

For this year, the team prepared a technology demonstrator consisting of only one glider deployed at apogee. This can be extrapolated for a fleet of 7 gliders. The challenge of building more gliders lies in fitting them into a constrained space in the rocket, and still equip them with advanced instrumentation for navigation and control.

Motivation for choosing this payload

Rovers such as Curiosity or Spirit have studied Martian terrain and sent back scientific data which may answer questions regarding the origin of life. However, in-situ atmospheric measurements of Mars on longer distances are missing. In order to solve this need, gliders, balloons, or powered planes should overfly Mars and land in areas where rovers cannot. Several projects are proposed by NASA in these directions such as the Preliminary Research Aerodynamic Design to Land on Mars (Prandtl-m) Airplane which aims to be released from a 3U CubeSat and do a 1-hour descent onto the surface of Mars.⁴

Inspired by the Prandtl-m project, our team aimed to design and build an autonomous glider for the

Spaceport America Cup competition, and learn more about the flight dynamics and control of such a complex system.

The payload shall weight 8.8 lb (4 kg).
The payload shall consist of a glider and ballast.
The glider shall be deployed at apogee.
The glider shall deploy its wings passively once ejected from the rocket.
The glider shall be equipped with an RTK (Real Time Kinematic) GPS used for navigation.
The glider shall be equipped with a COTS autopilot and a pitot tube
The glider's battery life shall be 1.5 hours.

Table 2: Top Level Requirements for the payload

III.ii Design and Manufacturing of one glider

Due to space constraints, the glider was chosen to be a flying wing with the wings folded in front. XFLR simulations with different airfoils, wing span, wing sweep were performed until the acceptable flight parameters were obtained. The final airfoil is a MH45, with improved (3%) reflex.

The plane parameters are presented in Table 3, while the optimal flight parameters are shown in Table 4.

wing span	0.72 [m]	2.36 [ft]
wing area	0.07 [m ²]	0.75 [ft ²]
mass	0.27 [kg]	0.61 [lb]
wing load	4.06 [kg/m ²]	0.83 [lb/ft ²]
root chord	0.11 [m]	0.36 [in]
neutral point	0.09 [m]	0.29 [in]
tip twist	-4°	
aspect ratio	7.50	
root-tip chord	21°	

Table 3: Plane parameters

speed	18.42 [m/s]
angle-of-attack	4.5°
lift coefficient (C_L)	0.21
drag coefficient (C_D)	0.02
C_L/C_D	10

Table 4: Flight parameters

The glider was designed in Solidworks. All the components of the glider are encapsulated either in

the fuselage, or in the wings, as it can be seen in Figure 15 and Figure 16.

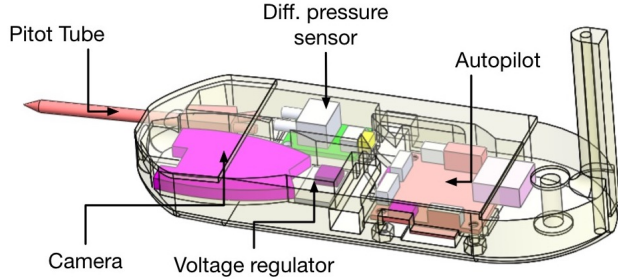


Fig. 15: Fuselage with components encapsulated

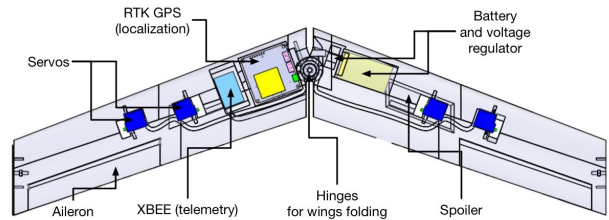


Fig. 16: Wings with components encapsulated

The wings are folded in front, as it can be seen in Figure 17. The unfolding mechanism is driven by a torsion spring. A set of magnets are used to keep the wings locked in the unfolded position. The force of the ejection springs on the rail is higher than the friction force of the glider's wings inside the box. Therefore no additional system to keep the wings folded was required and the wings were held folded by the walls of the payload box. The wings are placed one on top of each other, a decision taken in order to optimize the space in the cuboid and to add simplicity in design and manufacturing.

The second important part of the payload is the ejection system - the system that pushes the glider outside the rocket. The ejection system is placed in a 4U Cubesat standard cuboid made out of wood and reinforced with glass fiber. The system consists two rails, pulleys, string, spring and one servomotor for locking (Figure 18). The glider is ejected from the rocket by with a spring. The elongation of the spring is doubled using a system of pulleys so that the force can be applied over the whole length of the rail. A servomotor keeps the glider in place with a retractable pin that protrudes into the glider's fuselage block. With this rail-spring system, more gliders can be easily placed in the cuboid in the future.

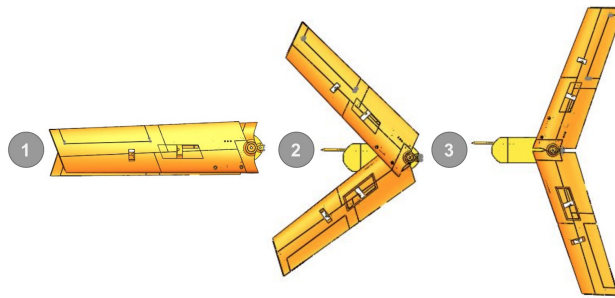


Fig. 17: Unfolding steps 1. The glider is fully folded in its bay. 2. The glider is ejected from the rocket and starts unfolding. 3. The glider is unfolded and starts flying back to the ground

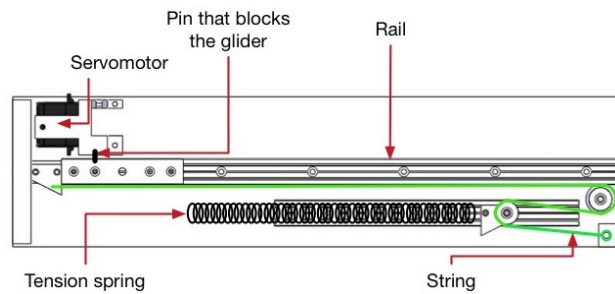


Fig. 18: Ejection System without the glider inside

The glider's wings and fuselage were 3d printed with thin walls and little infill to be lightweight and reinforced with carbon fibre and glass fibre (where GPS or telemetry antennas were placed). The manufacturing of one of the wings can be seen in Figure 19.



Fig. 19: Lamination of one of the glider's wings

Figure 20 shows the final design of the wing, as well as the ejection system cuboid.

Due to time constraints, this year's glider was not autonomously controlled. Below, the team proposes one navigation concepts that can be put in practice



Fig. 20: Final design of one glider

in the future rocket flights.

III.iii Navigation of the fleet of gliders

Gliders mounted inside a rocket are very challenging to be designed. Complex navigation instrumentation cannot be mounted on the gliders, due to space and weight constraints. We are thus proposing a solution of using GPS and Ultrawide band beacons for a formation flight of 3 gliders. Both sensors do not require a lot of space and do not weight much. The concept is as follows:

1. Ejection Phase: The gliders are ejected from the rocket at apogee
2. Find Phase: As the gliders might be spread in many directions, it is important to gather them in order to start the formation. For example, the module we propose (DWM1000) has an up to 290 meters communications range. Therefore, for this phase, GPS will be used to determine the position. Once the position is determined for all the 3 gliders, a leader is decided to be the glider closest to the other two. The leader will be thus followed by the other two.
3. Formation Phase: Once they are close to each other, the UWB beacons are used. They will measure the time of flight, thus the distance between each glider. The idea is to keep a constant distance between the leader and the other two gliders. The orientation of the formation is unknown. For this, we propose to use the barometer to keep a formation parallel to the ground.
4. Landing Phase: The landing shall be done in a net, to avoid crashing.

IV. RESULTS

The rocket RORO I flew twice. The first flight was a test flight in Switzerland and the second flight was the competition flight at Spaceport America Cup.

On board of the rocket there were an Inertial Measurement Unit (IMU) and a barometer that logged data to an SD card. This data has been analysed for both of the flights.

IV.i Rocket Test Flight

The test flight was performed in Kaltbrunn, Switzerland to a target apogee of 565m using an Aerotech K1275 motor and a lift-off mass of 18.3 kg. The apogee was limited to 600m due to proximity to buildings.

The rocket flight was successful, to an apogee of 502m, with two anomalies:

- The main parachute opened at apogee instead of at 200m above ground
- The rocket oscillated at a high angle of attack

The main chute opening cause has been identified from the high quality video of the optical tracking done by ETHZ. In conclusion, the parachute opening at apogee has been caused from the shock of the separated rocket stretching out the shock cord to the drogue parachute, where also the main chute bag was attached. This shock pulled the main chute cords out of the bag, which then pulled out the entire main chute.

This design problem has been fixed by securing the main chute cords in the bag until the chute is released.

The second anomaly, the oscillation and high angle of attack, required an analysis of the IMU data as the cause of the high angle of attack could not be identified simply from video footage.

IMU Data Analysis

In the following, the z-axis is the roll axis and points down along the rocket and the x and y-axes are pitch and yaw respectively.

The IMU on board the rocket was an MPU-6000 MEMS 3-axis gyroscope and 3-axis accelerometer from InvenSense.

The gyroscope measures angular rate which has to be integrated to obtain the attitude of the rocket. To reduce attitude drift due to high zero-rate bias of these MEMS gyroscopes, the bias was estimated by taking the average output while the rocket was on the launch rail from 30 seconds before lift-off to 5 seconds before lift-off. This should give a reasonably precise attitude for the approximately 10 seconds to apogee.

The accelerometer bias could not be calibrated on the launch pad, as the precise inclination of the

launch-rail was not known. Therefore the accelerometer was calibrated after the flight for scale and bias by sequentially placing the IMU on each of the six faces up. The bias for an axis is obtained by taking the mean between the averaged positive one g acceleration and averaged negative one g acceleration. The scale for the axis is obtained by taking the half of the difference between the positive and negative one g acceleration.

$$bias_i = \frac{a_i^{+g} + a_i^{-g}}{2} \quad [2]$$

$$scale_i = \frac{a_i^{+g} - a_i^{-g}}{2g} \quad [3]$$

After sensor calibration, the first step was to integrate the angular rate to obtain the attitude of the rocket. The attitude throughout the flight was visualized in 3D. In the animation the tilting and subsequent oscillation of the rocket was well visible, but the source of the disturbance was not evident.

The next step was to correct the calibrated IMU accelerations for centripetal and tangential accelerations due to angular rate and angular acceleration, as the IMU is not placed at the centre of mass. This gives us the acceleration at the centre of mass:

$$\mathbf{a}_{CM} = \mathbf{a}_{IMU} - \mathbf{a}_{tangential} - \mathbf{a}_{centripedal} \quad [4]$$

$$\mathbf{a}_{tangential} = \dot{\boldsymbol{\omega}} \times \mathbf{r}_{IMU}$$

$$\mathbf{a}_{centripedal} = -|\boldsymbol{\omega}_{tangential}|^2 \mathbf{r}_{IMU} \quad [5]$$

$$\boldsymbol{\omega}_{tangential} = \boldsymbol{\omega} - \frac{\boldsymbol{\omega} \cdot \mathbf{r}_{IMU}}{r_{IMU}^2} \mathbf{r}_{IMU}$$

where \mathbf{r}_{IMU} is the position of the IMU with respect to the centre of mass

The centre of mass location is obtained from the Solidworks CAD (which was experimentally verified for the lift-off configuration) and is linearly interpolated from lift-off configuration to burn-out configuration for the time of the motor burn. This is good enough, as the motor burn curve is quite constant.

This acceleration at the centre of mass was then used to compute the side-forces acting on the rocket using the known mass. Again the mass is interpolated during the burn as for the centre of mass.

With the assumption that the side forces are aerodynamic, they should act at the centre of pressure, which can be analytically determined. This results in a moment which was calculated using eq. 6.

$$M_x^{aero} = (z_{CP} - z_{CM})(-F_y) \quad [6]$$

$$M_y^{aero} = (z_{CP} - z_{CM})F_x$$

This aerodynamic moment was then compared with the actual moment that was acting on the rocket. The actual moment was obtained from the angular rates and the inertia by use of the Euler equations for rigid body dynamics. For an equal pitch and yaw inertia these equations are:

$$\begin{aligned} M_x &= I_{xy}\dot{\omega}_x + (I_z - I_{xy})\omega_y\omega_z \\ M_y &= I_{xy}\dot{\omega}_y + (I_{xy} - I_z)\omega_z\omega_x \\ M_z &= I_z\dot{\omega}_z \end{aligned} \quad [7]$$

The comparison between aerodynamic model based moments and actual moments is show in Figure 21.

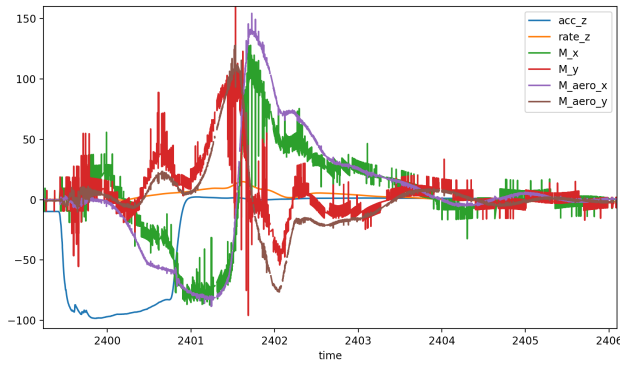


Fig. 21: Comparison of predicted aerodynamic moments (M_{aero_xy}) and actual moments (M_{xy}). The duration of the motor burn is clearly visible in the z acceleration. [accelerations in m/s^2 , rates in rad/s , torques in Nm]

The following observations are made:

- The moment after burnout and reduction of oscillations to reasonable angles of attack matches well with aerodynamic prediction. This validates our analytic centre of pressure determination.
- The moment after burnout but at high angles of attack is slightly lower than predicted by the aerodynamic model. This is to be expected, as the model does not include the cylindrical body lift which increases with angle of attack, moving the centre of pressure forward. A more forward centre of pressure would result in the smaller moments that were seen at high angle of attack.
- During the burn there is a permanent, about 20Nm mismatch between the aerodynamic prediction and the actual moments. After burnout this difference vanishes.

The first two points validated the aerodynamic model. They also showed that there was no torque acting on the rocket other the expected aerodynamic restoring torques at non-zero angle of attack.

The third point gives an important clue to the origin of the disturbance. For the duration of the motor burn, there was a moment that is not of aerodynamic origin. The best explanation is that this moment was caused by a misalignment of the motor thrust with respect to the centre of gravity.

A side accelerometer sensitivity to forward acceleration can be ruled out, as the side acceleration is around zero while accelerating on the launch rail. The same applies for the gyroscope that is close to zero until the rocket leaves the launch rail.

There are several possible causes for the thrust misalignment.

- The centre of gravity is not centred in the rocket
- The rocket motor is not centred in the rocket
- The rocket motor was not aligned with the rocket body
- The rocket body bent under load which place the CG out of the line of thrust
- The rocket motor was aligned, but produced a side-thrust.

With the K1275 motor the thrust misalignment which created a torque of 20Nm would correspond to an off-centre CG or off-centre motor mount of 15mm or a motor misalignment of 0.79 degree. Careful inspection and measuring of the rocket ruled out all the above mentioned possible causes except for the last one. Unfortunately we did not keep the nozzle, which is a consumable of the COTS motor assembly. Therefore it is impossible to check if any asymmetries are visible in the erosion of the nozzle.

Test Flight Analysis Conclusion

The high angle of attack during the test flight was caused by a thrust misalignment. The most probable explanation for the thrust misalignment seems to be a defect in the Aerotech K1275 COTS motor.

The reason for the lower apogee than the predicted one is due to the higher drag of the rocket flying at an angle of attack. Therefore it is important to dampen oscillations quickly so that the rocket minimizes the time where it is at a high angle of attack after a disturbance.

As a result of the conclusion of the IMU data analysis we were faced with a design trade-off. We

wanted to increase the damping of oscillations and at the same time increase the corrective force of the fins, to be able to withstand a potential thrust misalignment of a motor with more thrust than would be used for the competition flight. Unfortunately with an increase of corrective force of the fins, the damping ratio decreases, which increases the time to dampen oscillations.

As the exact source of the thrust misalignment could not be identified, we decided to sacrifice some of the damping and increase the corrective force of the fins to the maximum that was within the guidelines of the competition. For this, we increased the span of the fins by 30%. The resulting corrective force for a certain angle of attack was about doubled and the damping ratio went from 0.13 to 0.083. We estimated that this would give us enough safety to withstand a similar thrust misalignment angle with the stronger motor used at the competition.

IV.ii Rocket Competition Flight

The second flight of our rocket was at the competition at Spaceport America, New Mexico. The motor used was an Aerotech M2100, liftoff mass was 24.8kg and the predicted apogee was 3032m. The flight was successful with a reached apogee of 2738m.

At apogee, the rocket separated and started its descend on the drogue parachute. A few seconds later, the nosecone deployed and the glider payload was released successfully. At an altitude of around 460m the recovery avionics triggered the main parachute opening. The main parachute was successfully released from the parachute bag. Unfortunately it did not open as intended because the cords of the main parachute and the drogue parachute were entangled. This led to the top main parachute being pulled down, preventing it from inflating properly. Because of this, the touchdown velocity was with 30m/s too high for the rocket to survive undamaged.



Fig. 22: Landing site of the rocket

From the analysis of the landing site (see fig-

ure 22), especially the way the two parachute lines were entangled, we determined that the most likely cause of the entanglement was wrong packing of the parachute and shock cords. The hypothesis is that the drogue parachute was put in the parachute bay too loose and during handling of the rocket the the parachute moved around the shock cords of main parachute.

From the log files of the two recovery avionics we discovered that the primary recovery electronics did not detect the apogee and stopped working around four seconds after the drogue opening. The backup recovery electronics, which has a timer for the time-to-apogee and barometer for the main chute deployment worked without issues.

In terms of rocket flight performance the competition flight was satisfactory although there were some initial oscillations during the propulsive flight phase. These oscillations are probably the reason for the lower than predicted apogee.

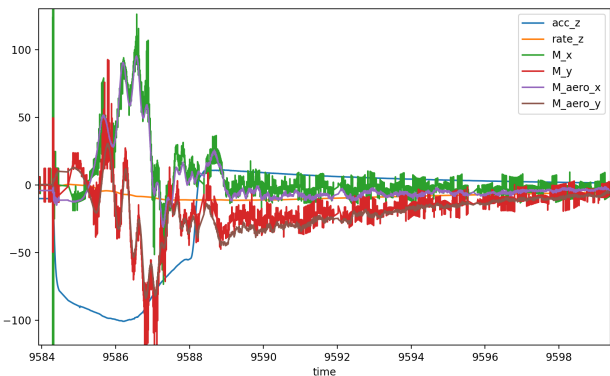


Fig. 23: Comparison of predicted aerodynamic moments (M_{aero_xy}) and actual moments (M_{xy}). Contrary to the test flight, for the competition flight the two curves match which means that there was no thrust misalignment present. [accelerations in m/s^2 , rates in rad/s , torques in Nm]

Unlike the test flight there was no thrust misalignment with the competition motor. As can be seen in Figure 23, the aerodynamic and actual moments match, indicating no thrust misalignment. In the figure, also the initial oscillations are visible. Our initial rocket design had lower than optimum damping and we decreased the damping even further after the test flight in order to maximize robustness against a potential thrust misalignment. Therefore the oscillations during the competition flight were only slowly damped.

For the source the disturbance that caused the oscillations we don't have clear evidence, but we suspect that the launch rail that guides the rocket for the first 5.5m could be an important factor. The launch rail we used was one that was provided by the competition organizers. It has a very thin construction and was bending slightly under the load of the rocket resting on it. (see Figure 24) The video of our camera next to the launch pad shows that the rail flexed slightly towards the rocket as the rocket lifts off the pad and no longer hangs on the rail. It is unsure if that would be sufficient to cause the oscillation of the rocket but we recommend to use a more stiff launch guide for the next year's rocket.



Fig. 24: Picture of the rocket taking off

IV.iii Glider Test Flights

The glider's flight was tested before the competition. However, the dropping altitude was maximum 100 meters, not 3048 meters, the expected apogee of the rocket.

The setup for testing the glider (Figure 26) was the following:

- A bigger plane with enough payload capacity to carry the glider was used
- The glider (Figure 26) was attached to the big plane using a string.
- The glider was deployed when desired, using a servomotor system that released the string.
- Two RC pilots were used, one to fly the big plane and one to fly the glider.



Fig. 25: The first prototype of the glider - used for testing



Fig. 26: The big plane carrying the glider for drop tests

IV.iv Glider Competition Flight

The glider was deployed at apogee, as planned. From the crash wreckage (Figure 27), we can see that the glider deployed its wings. As it had no autonomous control, when ejected from the rocket, it did not pitch up or stabilize its roll. Therefore, it can be assumed that it spiraled down until it crashed on the ground. The Pitot tube was found sticking in the ground, indicating a forward flight (Figure 28). Therefore the deployment system must have worked as intended, as the glider would not have flown forward in the folded configuration due to mass distribution. One of the wings was half-damaged, while the other one is in good condition. The fuselage was fully destroyed.



Fig. 27: The glider wreckage



Fig. 28: Pitot tube sticking in the ground which is evidence of the successful deployment

V. CONCLUSIONS

This paper presented a technology necessary to construct a rocket capable of achieving 10,000 ft altitude and land safely on the ground. With the absence of control, the stability of the rocket was guaranteed

by the extensive simulations done in 3 different simulators with one being developed by the team for the purpose of this project. The challenges with dynamic stability have also been explored and proper fins sizing done to dampen the oscillations. Throughout the subsystems presented, manufacturing process is also outlined to demonstrate the complete journey from the idea through the conceptual design to actual prototype.

The dual recovery process employed on the presented model composed of two parachutes and redundant electronics is capable of ensuring a safe landing even in presence of electronic faults. Custom made avionics, placed inside the nosecone of the rocket, provided necessary functionalities to control deployment of the payload and to log external parameters. It is designed to support further improvements such as air-brake or control system, possibly to be implemented in the following years.

Second part of the paper presented the glider constructed and placed inside the rocket as a payload. It has been deployed at the apogee with the goal of controlled landing on a fixed location and sending data to the ground station. Concepts for a fleet of autonomous gliders flying in formation and landing on a predefined position were also presented together with challenges in terms of navigation and control. Throughout the project, many tests have been performed on subsystem and system level to ensure compliance with requirements and to validate their functionalities, but due to the conciseness of this paper many results obtained are omitted.

Last but not least, Spaceport America Cup was a success for the Swiss team. The team was ranked 8th out of 83 teams flying rockets and 116 teams initially registered.

VI. OUTLOOK

The project presented above represents the first iteration and first prototype of both the rocket and the payload. The complete workload from the conceptual design to manufacturing has been done in the span of 7 months. Therefore, many of more advanced concepts which require time and thorough testing could not be implemented on this year's model. Some of those concepts are: implementation of the control system or the more simpler air brake system and the payload modifications to include the fleet of gliders. Even though they weren't implemented, many of these concepts have been researched and prototyped. The concept of the fleet of autonomous gliders has been presented in this paper, but also first iterations

of the air brake systems have been developed and tested on one of the smaller models of the rocket. The test of this system was performed in a wind tunnel and subsequently the prototype was launched in Kaltbrunn, Switzerland on May the 20th 2017. Figure 29 shows the smaller, so-called "Level 1" rocket with air brakes in a wind tunnel.



Fig. 29: Level 1 Rocket with Air Brakes in HEPIA Wind Tunnel

Following our success, there will be two Swiss teams participating at the competition next year, one from Swiss Federal Institute of Technology Lausanne (EPFL) and one from Swiss Federal Institute of Technology Zrich (ETHZ).

REFERENCES

- [1] S. A. Cup, "Intercollegiate rocket engineering competition rules & requirements document," tech. rep., 2017.
- [2] H. Arif, "Identification and control of a high power rocket," tech. rep., Ecole Polytechnique Federale de Lausanne (EPFL), 2017.
- [3] ESA, *ECSS Space Engineering*. ESA Requirements and Standards Division ESTEC, 2011.
- [4] NASA, "Could this become the first mars airplane?." https://www.nasa.gov/centers/armstrong/features/mars_airplane.html, June 2015.